

Experimental and Simulation Research on the Quasi-dynamic Extrusion Process of the Belt

Qi Liu *, Yuwei Wang, Wenfang Zh and Na Zhao

Northwest Institute of Mechanical and Electrical Engineering, Xianyang, China

Abstract. The extrusion process of the elastic belt is a process in which the elastic belt and the inner bore of the barrel undergo complex contact and collision, and the rifling gradually penetrates the elastic belt, so that the material of the elastic belt continues to fail and destroy. It has high instantaneous, strong impact, high temperature, high-speed change. There is a big gap between the existing theory and the actual squeeze-in process, and it is urgent to carry out research work on this problem. In this paper, a quasi-dynamic test device for the extrusion process of the elastic belt is established. On this basis, the extrusion history of a small-caliber projectile under different belt materials, different extrusion speeds, different extrusion force loading rates and different chamber pressure loading rates is established. The experimental comparison research was carried out. Based on the experimental data, the model calibration was carried out for the simplified chip resistance model of the belt extrusion process, and the calibration model was used to test the extrusion resistance of a newly designed large-caliber and howitzer belt extrusion process. The prediction research is carried out, which provides a reference for the optimal design of internal ballistics and charges, projectiles and barrels, and the coupling design of projectiles, guns and charges in a system.

key word: Belt, extrusion, quasi-dynamic, experiment

1. Introduction

When the artillery automatic weapon is fired, the projectile moves along the barrel under the action of high temperature and high pressure gunpowder and gas, and interacts with the barrel. The extrusion process of the elastic belt has an important impact on the internal ballistic cycle of the barrel weapon. In the classical internal ballistics, friction work and projectile rotational energy are often considered as secondary work and are included in the internal ballistic energy balance equation, and the extrusion process is ignored. When the pressure reaches the starting pressure, the projectile starts to move, which is quite different from the actual situation [1].

The extrusion process of the elastic belt is actually a process of contact and collision between the elastic belt and the inner bore of the barrel, the rifling gradually penetrates the elastic belt, and the material of the elastic belt continues to fail and destroy. The laws of advance resistance and elastic belt deformation are very complex [2-4]. Due to many difficulties, there is still a big gap between the existing research theories and the actual extrusion process, and it is urgent to carry out research work on the extrusion process.

The importance and complexity of the extrusion process make it a hot and difficult point in the research of launch technology. Many scholars are devoted to the model research of the extrusion process of the elastic belt, such

as the Johnson-Cook constitutive model [5]. With the help of three-dimensional simulation analysis software such as ABAQUS studies the large deformation of the elastic band, the plastic deformation flow process of the elastic band material, the shear failure process, and the groove formation process [6], and then study the projectile motion law, extrusion pressure, extrusion resistance change law. However, so far, there is no complete theory about the squeeze-in period in the ballistic literature at home and abroad, and scholars have not reached a consensus on the physical meaning of the squeeze-in pressure value, let alone a satisfactory squeeze-in resistance calculation. Methods [7-9]. With the help of 3D simulation software to calculate the intrusion resistance, the modeling process is complex, the number of parameters is large and difficult to determine, and the accuracy of the calculation results is difficult to grasp. In view of the above problems, this paper establishes a quasi-dynamic test device for the extrusion process of the elastic belt. Based on the experimental data, the simplified chip resistance model of the belt extrusion process was model calibrated, and the calibrated model was applied to the extrusion process of a newly designed large-caliber plus howitzer belt. The intrusion resistance is predicted and researched, which provides a reference for the optimal design of internal ballistics and charges, projectiles and

* Corresponding author: shamozhiying-67@163.com

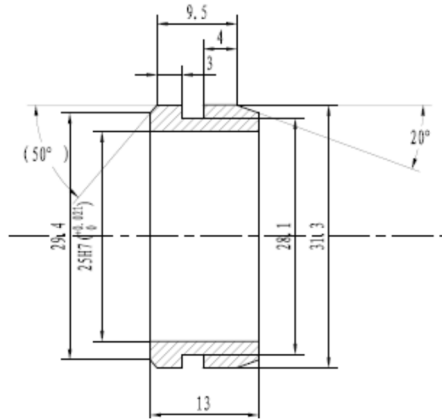
barrels, and the coupling design of projectiles, guns and charges in a systematic way.

2. Experimental research on the quasi-dynamic extrusion process of the belt

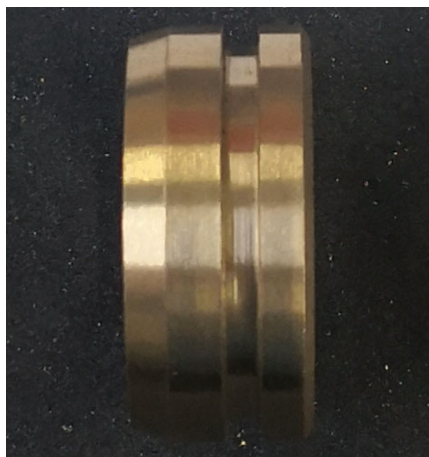
2.1 Introduction of Test Bench

2.1.1 Tested Product

The tested items are elastic belts of different structure sizes and materials. The design drawings of standard elastic belts (1#, material brass H96, first top surface width 4mm, chip groove width 2.5mm, belt forward inclination angle 20°) and The physical map is shown in Figure 1, and the material properties of different material elastic belts are shown in Table 1.



(1) Design drawing of the elastic belt



(2) Physical drawing of the elastic belt

Figure 1 Standard belt diagram

Table 1 Material properties of different elastic bands

material	material properties				
	density $\rho(kg / m^3)$	elastic modulus $E(GPa)$	poisson's ratio μ	strength limit $[\sigma](MPa)$	strength criterion
Brass H96	8900	115	0.34	320	Tensile strength
Duralumin 2A-12	2770	69	0.33	502	Tensile strength
Nylon 1010	1150	8.3	0.28	60	Tensile strength

2.1.2 Participating Products

The test items of this test bench are mainly simulated projectiles, truncated barrels and supports. Among them, the simulated projectile consists of a warhead, a tail and a simulated belt, as shown in Figure 2. When assembling, first put the elastic belt on the end of the warhead from the rear end, and then fasten the tail and the warhead through threads, and at the same time perform the axial positioning of the elastic belt, and then snap the simulated projectile into the rifling barrel as a whole. Since the warhead and the tail are separated and connected by threads, the elastic belts of different materials and different structural parameters can be replaced, and the influence of different material elastic belts and different elastic belt structure sizes on the intrusion resistance can be studied.

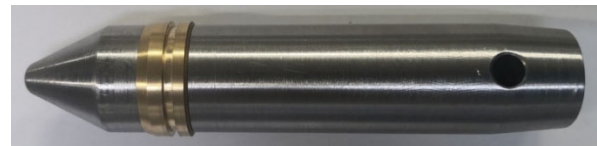


Figure 2 Assembly drawing of the belt and the simulated projectile

The truncated barrel is designed according to the structure and size of a small diameter barrel, as shown in Figure 3. The truncated barrel includes a complete sloped bore portion, a rifling start portion and a part of a full rifling portion. When assembling, the simulated projectile is snapped into the truncated barrel as a whole (apply a preload of about 200N). During the squeeze-in test, the design length of the tail should ensure that the notching of the elastic belt is completed and that the elastic belt part of the simulated projectile can completely pass through the truncated barrel. The support body is made of gun steel. Its function is to provide support for the shortening of the barrel during the extrusion process of the elastic belt, to ensure that the extrusion direction is along the axial direction of the barrel, and to provide a channel for simulating the movement of the projectile and play a soft recovery role. The whole test The physical drawing of the device is shown in Figure 4.



Figure 3 The actual picture of the truncated body tube



Figure. 4 The actual picture of the assembly of the extrusion test device

2.1.3 Power Loading Mechanism

The loading mechanism of the intrusion force is a computer-controlled universal testing machine, and its main parameters are: model: 105D; maximum test force: 100KN; displacement resolution: 0.025 μ m; test force resolution: 1/500000FS; sampling frequency 30HZ.

2.1.4 Test Plan

The experimental protocol is shown in Table 2.

Table 2 Test Embodiments

test item	squeeze working condition				test quantity		test content
	band material	extrusion force loading rate (KN/s)	chamber pressure loading rate (MPa/s)	extrusion speed (mm/s)	single	accumulative	
material comparison	H96 brass	—	—	—	3	3	F-L、 F-t、 L-t、 weighing 、 ordinary photography (video)
	duralumin 2A-12	—	—	—	3	6	
	nylon1010	—	—	—	3	9	
squeeze speed contrast	—	2	—	—	3	12	
	—	4	—	—	3	15	
	—	6	—	—	3	18	
	—	8	—	—	3	21	
intrusion force loading rate comparison	—	—	0.5	—	3	24	
	—	—	1	—	3	27	
	—	—	1.5	—	3	30	
	—	—	2	—	3	33	
	—	—	2.5	—	3	36	
chamber pressure loading rate comparison	—	—	—	20	2	38	
	—	—	—	30	2	40	
—	—	—	40	2	42		

2.2 Analysis of Test Results

2.2.1 Comparison of the Extrusion Process of Different Belt Materials

Figure 5 shows the comparison of elastic belts of different materials before and after extrusion. It can be seen from Figure 5 that the elastic belt of nylon Nylon1010 only undergoes elastic deformation of the material before and after extrusion, and no chips are formed; while the duralumin 2A-12 material The hardness is relatively high. Although the chip deformation occurs, the chip material of the elastic belt is not adhered to the elastic belt and the simulated projectile. Soft, copper scraps accumulate in the chip slot after the extrusion is completed, and the copper hanging on the rifling is more serious. When the projectile passes through the fully-rifled barrel, there are obvious traces of copper hanging on the outer wall of the projectile circumference. This phenomenon can also be explained. , using the brass H96 material belt, when designing the charge, the copper remover should be used as the charge accessory.



(1) Comparison before and after the brass H96 material belt is squeezed in



(2) Comparison of before and after extrusion of duralumin 2A-12 material belt



(3) Comparison of nylon Nylon1010 material belt before and after extrusion

Figure 5 Comparison of elastic belts of different materials before and after extrusion

Figure 6 is a comparison of the typical extrusion resistance curves of the three elastic belt materials. It can be seen from Figure 6 that the extrusion resistance curve of the standard brass H96 elastic belt is obviously bimodal, and the resistance peak value when passing through the second top surface Higher than the peak value of the first top surface; the extrusion resistance curve of the duralumin 2A-12 elastic belt is single-peaked, and the resistance curve has an inflection point when passing through the first top surface; the extrusion resistance curve of the nylon Nylon1010 elastic belt is double-

peaked. And the first peak is higher than the second peak. It can be seen from the three extrusion resistance curves that the peak extrusion resistance is duralumin 2A-12>brass H96>nylon Nylon1010.

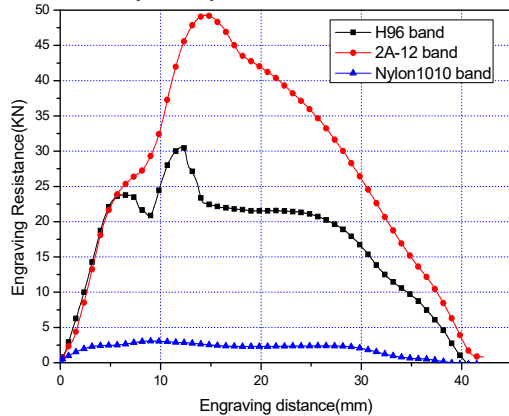


Figure 6 Comparison of intrusion resistance curves at of belts of three materials

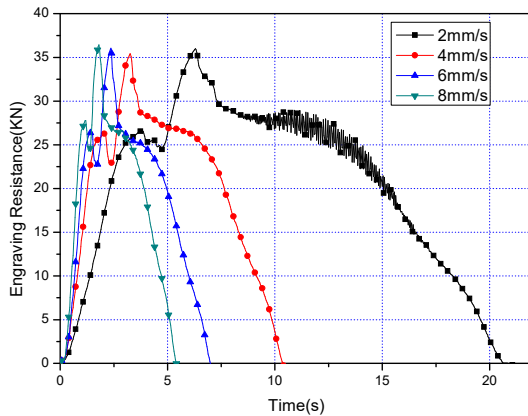


Figure 7 Comparison of intrusion resistance different extrusion speeds

2.2.2 Comparison of Extrusion Resistance Curves at Different Extrusion Speeds

Set the extrusion speed to 2mm/s, 4mm/s, 6mm/s, and 8mm/s respectively. Figure 7 shows the comparison of the extrusion resistance curves at different extrusion speeds. It can be seen from Figure 7 that at different extrusion speeds The shape of the extrusion resistance curve is similar, and the peak value of the resistance curve is almost the same, and the difference is only in the completion time of extrusion.

2.2.3 Comparison of Intrusion Resistance Curves at Different Intrusion Force Loading Rates

Figure 8 shows the comparison of the intrusion resistance curves when the loading pressure at the bottom of the projectile increases according to the law of 500N/s-2500N/s. It can be seen from Figure 8 that with the increase of the intrusion dynamic loading rate, the peak value of the intrusion resistance curve There is a slight downward trend, and with the decrease of the extrusion dynamic loading rate, the extrusion process of the elastic

belt becomes more and more unstable, and the extrusion resistance curve shows obvious oscillations.

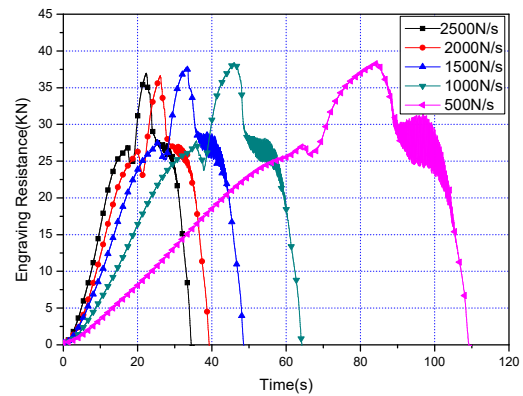


Figure.8 Comparison of intrusion resistance curves under different cavity pressure loading rates

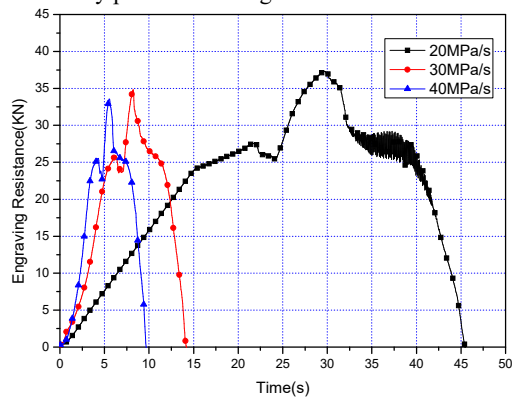


Figure.9 Comparison of intrusion resistance curves under different intrusion dynamic loading rates

2.2.4 Comparison of Intrusion Resistance Curves at Different Chamber Pressure Loading Rates

Figure 9 shows the comparison of the intrusion resistance curves when the chamber pressure loading rate increases according to the law of 20MPa/s-40MPa/s respectively. The peak value of the extrusion resistance curve decreased from 37.5kN at 40MPa/s to 28kN at 20MPa/s, a decrease of about 25.3%, and with the decrease of the chamber pressure loading rate, the extrusion process of the elastic belt became more and more unstable, and the extrusion process became more and more unstable. The resistance curve shows obvious oscillation at 20MPa/s, which is consistent with the changing trend under different extrusion pressure loading rates.

3. Research on simplified chip extrusion resistance model

3.1 Mathematical Model of Contact Stress

Two-dimensional deformation is described by the plastic theory equations:

$$\begin{aligned} \frac{\partial \sigma_x}{\partial x} + \frac{\partial \tau_{xy}}{\partial y} &= 0 \\ \frac{\partial \sigma_y}{\partial y} + \frac{\partial \tau_{xy}}{\partial x} &= 0 \\ (\sigma_x - \sigma_y)^2 + 4\tau_{xy}^2 &= \frac{4}{3}\sigma_\Phi^2 \\ u_x &= \lambda_1(\sigma_x - \sigma_{cp}) \\ u_y &= \lambda_1(\sigma_y - \sigma_{cp}) \\ \dot{\gamma}_{xy} &= 2\lambda_1\tau_{xy} \end{aligned} \quad (1)$$

By solving these equations, the contact stress calculation model is obtained:

$$\sigma_k = \frac{\bar{m}}{\gamma} \left[\left(1 + \gamma \frac{\sigma_{k,0}}{m} \right) \left(1 - \frac{tg\alpha_k}{h_0} x \right)^\gamma - 1 \right] \quad (2)$$

The contact stress is described as follows for different body sections:

(1) First slope:

$$\sigma_k = \frac{\bar{m}}{\gamma_1} \left[\left(1 + \gamma_1 \frac{\sigma_{k,0}}{m} \right) \left(1 - \frac{tg\alpha_{k,1}}{h_0} \cdot x \right)^{\gamma_1} - 1 \right] \quad (3)$$

(2) Second slope :

$$\sigma_k = \frac{\bar{m}}{\gamma_2} \left\{ \left(1 + \gamma_2 \frac{\sigma_{k,1}}{m} \right) \left[1 - \frac{tg\alpha_{k,2}}{h_1} (x - H_1) \right]^{\gamma_2} - 1 \right\} \quad (4)$$

(3) After entering the cylindrical part of the barrel (IV area), the contact stress is constant, on the negative line, and on the positive line:

$$\sigma_{k,1}^1 = \sigma_{k,1} - \bar{m} \cdot \alpha_{k,1} \quad (5)$$

$$\sigma_{k,2}^1 = \sigma_{k,2} - \bar{m} \cdot \alpha_{k,2} \quad (6)$$

According to the structural parameters of a small-caliber artillery barrel, projectile, and belt, as well as the material parameters of brass H96 (Table 3-Table 4), the contact area S_i between the barrel and the belt can be obtained.

According to the contact area between the elastic belt and the inner bore of the barrel and the contact stress acting on the area, the following contact resistance model is obtained:

$$F_{BP} = \mu \cos \alpha_k \left(1 + \frac{tg\alpha_k}{\mu} \right) \int_0^{S_k} \sigma_k \cdot dS_k \quad (7)$$

Among them, F_{BP} is the sum of the embedded resistance.

Assuming that the contact stress on the contact area between the elastic band and the barrel is uniform at the same slope, (10) can be further simplified as:

$$F_i = \mu_i \cos \alpha_{k,i} \left(1 + \frac{tg\alpha_{k,i}}{\mu_i} \right) \sigma_{cp,i} \cdot S_i \quad (8)$$

The total embedded resistance is determined by the sum of the stroke resistance of each segment: $F_{BP} = \sum F_i$. When the insertion section is composed of a smooth groove, a rifling slope and a cylindrical section (of the

rifling), the insertion resistance is the sum of three components: the first slope resistance F_1 , the second slope resistance F_2 and the cylindrical section resistance F_3 . According to the quasi-static intrusion test data of the elastic belt in the previous section, the prediction model of the intrusion resistance in the simplified chip process is obtained through multivariate regression of parameters. The strength parameters of brass H96 are shown in Table 3-4:

$$F_{BP} = \mu \cos \alpha_k \left(1 + \frac{tg\alpha_k}{\mu} \right) \frac{\bar{m}}{\gamma} \left\{ \left(1 + \gamma \frac{\sigma_k}{m} \right) \left[1 - \frac{tg\alpha_k}{h} (x - H) \right]^\gamma - 1 \right\} S_k \quad (9)$$

Table 3 Strength coefficient values of brass H96

ε_0	0	0.05	0.1	0.15	0.2	0.3	0.4	0.5	0.6
$\sigma_r^*/(kgf/mm^2)$	8.5	16	21	25	27	30	32	33.5	34.7
\bar{n}	14.7	5.93	3.43	1.36	0.89	0.47	0.28	0.18	0.12

Table 4 Material properties of brass H96

material	material properties				
	density $\rho(kg/m^3)$	elastic modulus $E(GPa)$	poisson's ratio μ	strength limit [σ](MPa)	strength criterion
Brass H96	8900	115	0.34	320	tensile strength

4. Research on prediction of squeeze-in resistance of a large-caliber howitzer

On the basis of simplifying the calibration of the intrusion model in the chip process, this model is used to study the intrusion resistance of a newly designed large-caliber and howitzer projectile in the intrusion process. The structural parameters and material properties used in the calculation are shown in Table 5. , the calculated contact area changes with the extrusion process are shown in Table 6, and the extrusion resistance and the extrusion component force with the extrusion process are shown in Table 7.

Table 5 Structural parameters and material properties of a large-caliber howitzer

name	symbol	unit	value
belt outer diameter	d_0	mm	163.8
yin wire diameter	d_H	mm	159.54
projectile stripping belt outer diameter	d_k	mm	153.8
band width	Hnp	mm	36.458
sunline tooth width	a	mm	3.81
yin line tooth width	B	mm	6.332
number of rifling	n_H	1	48
first slope angle	$\alpha_{k,1}$	rad	0.0495
second slope angle	$\alpha_{k,2}$	rad	0.018
the first slope bore considers the tangential stress action coefficient	ξ_1	1	1.0
the second slope bore considers the tangential stress action coefficient	ξ_2	1	1.0
plastic coefficient of elastic band material	$2K$	kgf / mm ²	22
material strength factor	\bar{n}	1	4.5
the friction coefficient of the first groove	μ_1	1	0.093
the friction coefficient of the second groove	μ_2	1	0.2
gunpowder gas pressure acting on the belt	P_n	MPa	0
first slope height	H1	mm	11.85
second slope height	H2	mm	89.15
rifle height	t	mm	2.3

Table 6 Variation of the contact area with the insertion stroke during the extrusion process of a large-caliber plus howitzer projectile

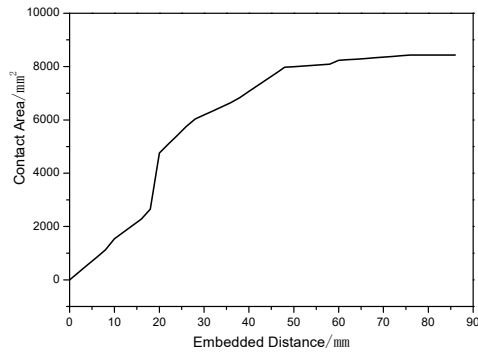
feature section	x / mm	S_k / mm^2	S_1		S_2		S_3	
			mm ²	%	mm ²	%	mm ²	%
0	0	0	0	0	0	0	0	0
0.5H1	5.925	1485	148 5	10 0	0	0	0	0
H1	11.85	4591	459 1	10 0	0	0	0	0
0.5Hnp	18.22 9	1257	125 7	10 0	0	0	0	0
0.5(H1 + Hnp)	24.15 4	3296	329 6	10 0	0	0	0	0
Hnp	36.45 8	2513	251 3	10 0	0	0	0	0
Hnp+0.5 H1	42.38 3	5980	560 3	93 .7	185 .5	3. 1	191 3.	3. 19
H1+ Hnp	48.30 8	6722	0	0	593	8. 82	612 9	91 .2
H1+0.5 (H2+ Hnp)	74.65 4	7970	0	0	123 7	15 .5	673 3	84 .5
H1+ H2	101	8218	0	0	123 7	15 .1	698 1	84 .9
H2+0.5 (H1+ Hnp)	113.3 04	8094	0	0	123 7	15 .3	685 7	84 .7
H2+ Hnp+0.5 H1	131.5 33	8321	0	0	927 .6	11 .1	739 3	88 .8
H1+ H2+ Hnp	137.4 58	8446	0	0	0	0	844 6	10 0
> H1+ H2+ Hnp	138	8446	0	0	0	0	844 6	10 0

Table 7 Variation of total intrusion resistance and resistance component of a certain caliber plus howitzer with embedded stroke

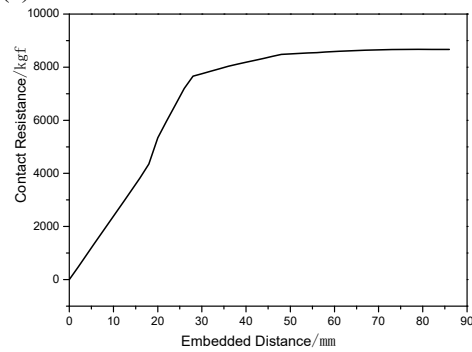
x / mm	F_{BP} / kgf	F_1		F_2		F_3	
		kgf	%	kgf	%	kgf	%
0	0	0	0	0	0	0	0
5.925	2138	2138	100	0	0	0	0
11.85	2269	2269	100	0	0	0	0
18.229	4276	4276	100	0	0	0	0
24.154	4682	4682	100	0	0	0	0
36.458	5027	5027	100	0	0	0	0
42.383	7629	4798	62. 9	577	7.56	2254	29.5 4
48.308	8071	0	0	3844	47.6 3	4227	52.3 7
74.654	8475	0	0	3844	45.3 6	4631	54.6 4
101	8574	0	0	3844	44.8 3	4730	55.1 7
113.304	8578	0	0	3844	44.8 1	4733	55.1 8
131.533	8646	0	0	2883	33.3 4	5763	66.6 6
137.458	8668	0	0	0	0	8668	100
138	8668	0	0	0	0	8668	100

The calculation results of Table 6 and Table 7 are shown in Figure 10. It can be seen that the contact area continues to increase with the extrusion process. At the beginning of the extrusion process, the contact area increases rapidly, and then grows slowly until the end of the extrusion process. , the contact area almost no longer increases, indicating that the extrusion process is completed, and the elastic belts have been embedded in the rifling of the cylindrical part of the barrel; and the extrusion resistance also shows a similar change rule to the contact area, that is, in the early stage of extrusion, the total contact resistance is rapid. Growth, followed by slow growth, to the basic level of the late extrusion curve, indicating that the extrusion resistance is no longer increasing, and the entire belt has entered the cylindrical rifling area. It can also be seen from Figure 10 that the extrusion force F1 in the first groove area is established first, and it is also the main part of the total extrusion resistance in the early stage of extrusion, but when the elastic belt extrusion distance exceeds about 37mm (this distance It is about the sum of the height of the first groove and the width of the elastic belt), and it quickly decays to 0, indicating that the elastic belt has completely passed the first groove area; at this time, the second groove is squeezed into the resistance component F2 and the cylindrical rifling area is squeezed The advancing resistance component force F3 has been established, and the extrusion component force of the second slope bore area only exists in the range of about 20mm to 75mm of the extrusion process, that is, only at this stage, the second slope bore and the bullet have contact stress . The contact stress of the rifling in the cylindrical part of the barrel is established when the extrusion process reaches about 20mm, and it increases continuously with the extrusion process, indicating that the contact area between the elastic belt and the rifling continues to increase. When the extrusion process is completed, the extrusion process is completed. The resistance component F3 basically no longer increases. From the extrusion resistance curve of the entire projectile extrusion process, the bottom pressure converted by the maximum extrusion resistance is 4.81MPa, which is much

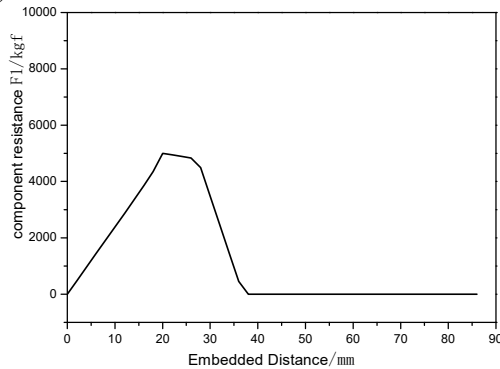
smaller than the starting pressure of 20MPa defined by the classical internal ballistics.



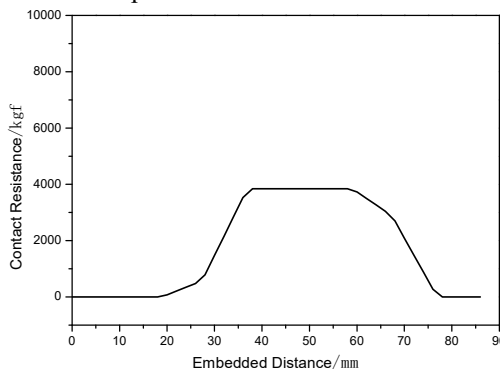
(a) Curve of contact area with insertion stroke



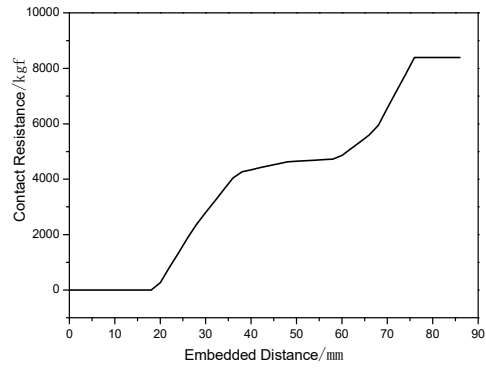
(b) Curve of insertion resistance with insertion stroke



(c) Curve of the resistance force component F1 with respect to the insertion stroke



(d) Curve of the resistance component F2 with the insertion stroke



(e) Curve of the resistance force F3 with the insertion stroke

Figure 10 Contact area and squeezing resistance change with insertion stroke

5. Conclusion

In this paper, a quasi-dynamic test device for the extrusion process of the elastic belt is established. On this basis, the extrusion history of a small-caliber projectile under different belt materials, different extrusion speeds, different extrusion force loading rates and different chamber pressure loading rates is established. The experimental comparison research was carried out. Based on the experimental data, the model calibration was carried out on the simplified chip resistance model of the belt intrusion process by using the multivariate parameter regression method. The process intrusion resistance curve was predicted and studied, and the following conclusions were obtained:

(1) The material dynamic behavior of elastic belts of different materials is quite different during the extrusion process. The nylon Nylon1010 elastic belt only undergoes plastic deformation, while the duralumin 2A-12 elastic belt produces brittle chips, and the brass H96 elastic belt produces plasticity at the same time. Deformation, brittle chips and viscoplastic deformation, therefore, the phenomenon of copper hanging on the rifling is more serious.

(2) The shape of the intrusion resistance curve is similar at different intrusion speeds, and the peak value of the resistance curve is almost the same, the difference is only in the completion time of the intrusion; with the increase of the intrusion dynamic loading rate, the peak value of the intrusion resistance curve is slightly different. With the decrease of the loading rate of the extrusion force, the extrusion process of the elastic belt becomes more and more unstable, and the extrusion resistance curve shows obvious oscillation; with the increase of the loading rate of the chamber pressure, the peak value of the extrusion resistance curve The peak value of the extrusion resistance curve decreased from 37.5KN at 40MPa/s to 28KN at 20MPa/s, a decrease of about 25.3%, and with the decrease of the chamber pressure loading rate, the extrusion process of the elastic belt became more and more unstable. , the extrusion resistance curve shows obvious oscillation at 20MPa/s.

(3) Under the same working conditions, the extrusion resistance curve is consistent during the extrusion process

of the elastic belt, and the peak consistency of extrusion resistance is good, but under different working conditions (when the structural parameters and extrusion force loading methods are different) The resistance curves are quite different.

(4) From the extrusion resistance curve of the entire projectile extrusion process, the bottom pressure converted by the maximum extrusion resistance is 4.81MPa, which is much smaller than the starting pressure defined by the classical inner ballistics 20MPa.

References

1. WAND Peng, YANU Guolai, GE Jianli, et al. Numerical simulation of rotating band engraving process based on Johnson-Cook constitutive model[J]. Journal of Ballistics, 2015,27(2):55-61. (in Chinese)
2. MA Mingdi, CUI Wanshan, ZENG Zhiyin, et al. Engraving process analysis of projectiles based on coupling of FEM and SPH[J]. Journal of vibration and shock, 2015,346(6):146-150. (in Chinese)
3. MA Mingdi, CUI Wanshan, ZENG Zhiyin, et al. Dynamic Response Analysis of Chamber Throat in the Engraving Process of Heavy Caliber Gun Projectile, Journal of North University of China(Natural Science Edition) , 2014, 35(3):263-269. (in Chinese)
4. WANG Liang-kuan, Liu Yi, Zhou Yu, Liu Tie-jun, Diwu Qiang-Qiang, Numerical Simulation of the Engraving Process of Pure Iron Rotating Band [J].Journal of Gun Launch & Control, 2018,39(152), 04 52-55+61. (in Chinese)
5. E.B. Culbanov, Yang Jingrong, Zhou Yanhuang. Ballistics and squeeze-in pressure calculation during squeeze-in period [M]. Beijing: National Defense Industry Press, 1997.
6. ZHUANG Zhuo, Nonlinear Finite Elements for Continua and Structures[M]. Tsinghua University Press, 2002. (in Chinese)
7. G.R. Liu, M.B. Liu, Smoothed Particle Hydrodynamics: A Meshfree Particle Method, World Scientific Publishing, 2003
8. Luca Massidda, Yacine Kadi, SPH simulation of liquid metal target dynamics, Nuclear Engineering and Design 240 (2010) 940–946
9. G. R. Johnson and W. H. Cook, A constitutive model and data for metals subjected to large strains, high strain rates and high temperatures. Proc. 7th Int. Symp. on Ballistics, pp. 541-547. The Hague, The Netherlands (April 1983).